Received 10 December 2022; accepted 22 December 2022. Date of publication 30 December 2022; date of current version 23 January 2023.

Digital Object Identifier 10.1109/OJAP.2022.3233260

Spectrum-Aware Compact Reconfigurable UHF Antenna for Interweave Cognitive Radio

F. A. ASADALLAH, H. ABDUL KHALEK, B. ABOU ALI MODAD, J. ABOUL HOSN, J. COSTANTINE (Senior Member, IEEE), R. KANJ (Senior Member, IEEE), AND Y. TAWK (Senior Member, IEEE)

Electrical and Computer Engineering Department, Maroun Semaan Faculty of Engineering and Architecture, American University of Beirut, Beirut 1107 2020, Lebanon

CORRESPONDING AUTHOR: J. COSTANTINE (e-mail: jcostantine@ieee.org)

This work was supported by the American University of Beirut, University Research Board.

ABSTRACT This paper presents a compact ultra-high frequency (UHF) folded antenna design that relies on a single radio frequency micro-electro-mechanical switch (RF-MEMS) to reconfigure its frequency of operation between 575 MHz and 760 MHz. The reconfigurable multi-layered antenna design has a volumetric folded topology with total dimensions of $40\times40\text{mm}^2$; equivalent to $0.11\lambda\text{x}0.11\lambda$ at 575 MHz. The antenna is fabricated and tested where the measurements agree well with the simulation results. The antenna exhibits a radiation efficiency of 40% at 575 MHz and 62% at 760 MHz. Furthermore, the proposed antenna is tested in a cognitive radio environment to validate its ability to adapt to cognitive input and tune its performance across white space within the UHF band. This is achieved by relying on a trained classifier model that is embedded within a microcontroller to autonomously control the state of the integrated switch based on which channel is idle.

INDEX TERMS Cognitive radio, miniaturization, reconfigurable antennas, RF MEMS, small antenna.

I. INTRODUCTION

COGNITIVE radio has emerged as a solution to ensure spectrum usage efficiency for modern communications. More specifically, interweave cognitive radio is a mode of operation where the spectrum is continuously sensed for available idle bands. Once these bands are identified, a processor reconfigures a communicating antenna to operate across these frequencies. As a result, the integration of a dynamic communication system within any cognitive radio platform is a necessity. Such dynamic communication can be achieved by implementing reconfigurable antenna components [1], [2], [3].

Reconfiguring an antenna necessitates the integration of components such as RF-MEMS, PIN diode switches, digitally tunable capacitors, or mechanical actuation mechanisms. Moreover, reconfigurable antennas designed for cognitive radio integration must be compact and optimized for swift and efficient communication. Various techniques that aim at reducing the physical size of the antenna without compromising its radiation characteristics are proposed in the literature [4], [5], [6], [7]. However, reconfiguring compact antenna elements present an additional challenge in cognitive radio front-end platforms that must be addressed. To that end, we propose a new multilayered folded compact reconfigurable antenna for integration in an interweave cognitive radio platform. The antenna, briefly introduced in [8], operates across two UHF bands: 575 MHz and 760 MHz, respectively. It is based on a multilayered structure to achieve the required compactness. The frequency reconfiguration is obtained by placing a single RF-MEMS between the loop and three integrated vertical folds.

The novel aspect of the presented design lies in its ultra-compact volumetric profile, which is considered advantageous for implementation in any portable miniature communication device for interweave cognitive radio across UHF TV bands. In addition, the folded multi-layered meandered loop structure combined with a dual-band impedance matching network adds to the novel aspects of the presented work. Moreover, additional novelty is based on the practical implementation of the antenna in an actual interweave cognitive radio scenario by relying on a pre-designed channel occupancy model. The channel occupancy model identifies available frequency bands and tasks the antenna to reconfigure its operating frequency to occupy these idle frequencies.

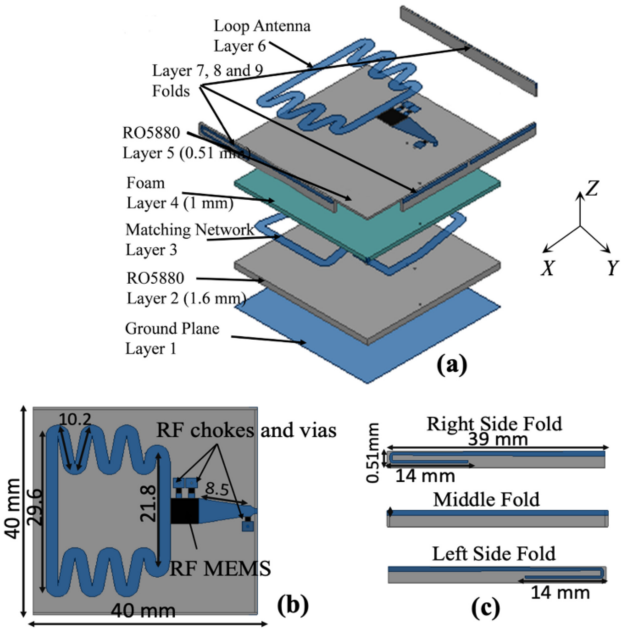

FIGURE 1. (a) The different layers of the proposed antenna structure, (b) The dimensions of the main radiating element along the RF chokes and vias used for biasing the RF MEMS, and (c) The three vertical layers with the meandered lines.

This mode of operation ensures that even if the spectrum is congested around some frequency bands, other idle bands are available and can be leveraged to always ensure continuous reliable communication. All these novel features prove that this antenna stands the tests and challenges of a cognitive radio channel.

Section II presents the multilayered folded miniaturized reconfigurable antenna along with the design of the proposed matching network. The full antenna prototype and the corresponding measurement results are presented in Section III. Section IV discusses the cognitive radio analysis and the prediction of channel availability. Section V concludes the paper.

II. PROPOSED DESIGN

The proposed multilayered folded design that is reconfigured by relying on a single RF-MEMS is shown in Fig. 1(a). It is composed of six planar layers and three vertical layers. Layer 1 is a 40 x 40 mm^2 ground plane. Layer 2 is the Rogers RO5880 substrate with a thickness of 1.6 mm. Layer 3 contains the dual-band impedance matching network that ensures matching on-demand at the two reconfigurable frequency bands. Layer 4 is a 1 mm thick foam substrate. Layer 5 is another Rogers RO5880 substrate of 0.51 mm thickness. Layer 6 is the meandered loop antenna.

The RF-MEMS is chosen versus a PIN diode due to its linear behavior, less power consumption, and higher radiation efficiency [9]. The RF MEMS is also incorporated within this layer along with its corresponding biasing network and its connection with the three vertical layers. More specifically, the three vertical layers, highlighted in Fig. 1(a) as layers 7, 8, and 9 folds, are composed of extended meandered lines to further increase the electrical length of the main radiating element. The proposed structure allows the antenna to feature total dimensions of 40 x 40 mm^2 with a thickness of 3.08 mm. The area of the structure is equivalent to 0.11λ x 0.11λ mm^2 at 575 MHz. These dimensions indicate a 70% size reduction at 760 MHz and 80% at 575 MHz in comparison to a patch antenna operating at the same frequencies.

The radiating structure, shown in Fig. 1(b), is a single loop element that is designed with its circumference corresponding to $\lambda_g/2$ at 760 MHz [10]. Its meandered shape is used to maximize the electrical length and achieve a compact design. The width of the line composing the loop is taken to be 2.1 mm which is translated into a characteristic impedance of 125 ohms. The loop has four meandering turns on each side. These dimensions ensure an operation at the first band of interest, which is 760 MHz. Achieving an operation at the second band (*i.e.,* 575 MHz) requires a further increase in the antenna's electrical length while while maintaining the same 40 x 40 x 3.08 mm^3 volumetric dimensions. Hence, an RF-MEMS (ADG901 [11]) is integrated within the radiating element as shown in Fig. 1(b). The switch connects the main meandered loop to the three vertical layers respectively. These three layers, highlighted in Fig. 1(c), are placed vertically at the three sides of layer 5.

The position of the RF-MEMS, highlighted in Fig. 1(b), is chosen to enable operation at 575 MHz and 760 MHz on demand. Accordingly, a dedicated feeding network, Layer 3 in Fig. 1(a), is designed to enable impedance matching at both frequencies. The corresponding layout of the integrated matching network is shown in Fig. 2(a).

The feeding network of the antenna is initiated with a 50-ohms coaxial connector that is fed into the matching network at layer 3. The state of the integrated RF MEMS affects the input impedance of the antenna as it enables its operation at two distinct frequencies. This effect results in the antenna behaving as two different loads respectively. A typically integrated quarter wavelength transformer cannot match different loads at different frequencies to a 50 Ω RF feed. A tuned shunt stub of the matching network can however solve this problem and alleviate the mismatch. The tuned shunt stub shown in Fig. 2(b) matches the antenna to two different frequencies and for a variety of loads. The proposed matching network is presented in Fig. 2(a) for both antenna impedance states. When the RF MEMS is ON, the antenna input impedance is $Z_{ON} = 60 + j60\ \Omega$. When the RF MEMS is OFF, its input impedance is $Z_{OFF} = 1.09 + j8.32\ \Omega$. An L-matching network is first designed for the two switch states separately.

To reach an acceptable impedance matching for both cases, the final transmission line (TL) and the final shunt stubs are chosen such that both impedances lie within the VSWR<2 circle on a smith chart, for a 50Ω input impedance. The final resulting network is optimized to match the two input impedances. As a result, it is composed of a shunt stub of 90 mm and a series transmission line of 110 mm in length. These dimensions of the final TL and the final shunt stub transform both Z_{OFF} and Z_{ON} into impedances that are located inside the VSWR=2 circle of the 50 ohms input on

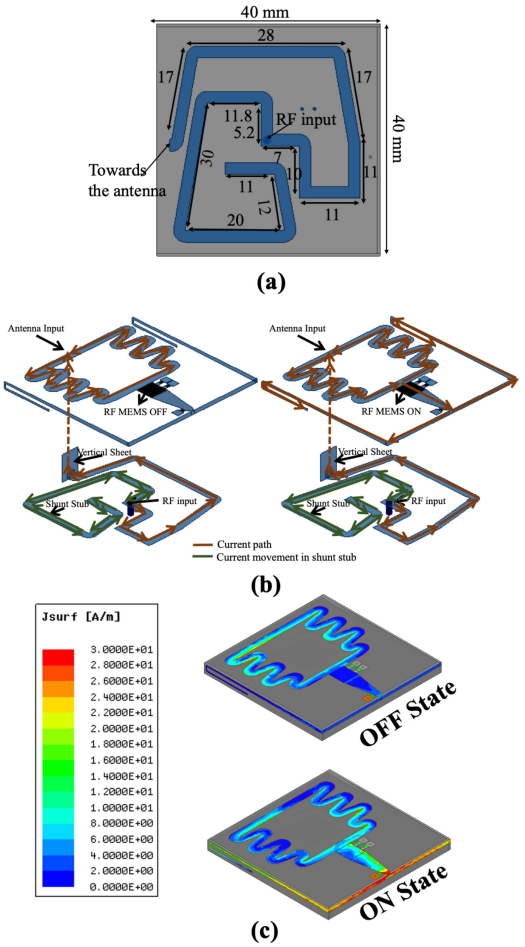

FIGURE 2. (a) The designed matching network (b) The current path for the two states of the integrated RF-MEMS along its biasing circuitry, (c) The corresponding surface current distribution along the radiating element and the three vertical layers for both states of the switch.

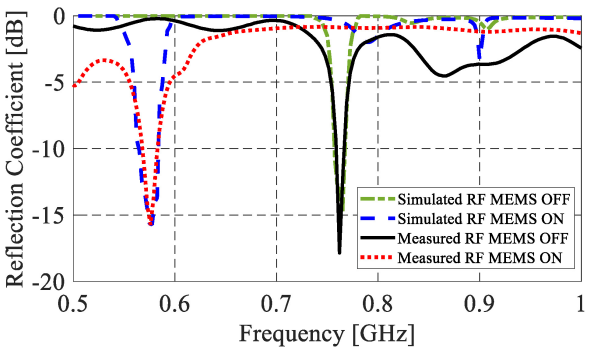

FIGURE 3. The simulated and measured reflection coefficients in dB for different switch states.

a smith chart. This proves that this network matches both impedances to the same 50 Ω input.

The matching network is also linearly folded in a spiral shape to reduce its size and ensure its lodging within the 40 x 40 mm^2 surface underneath the meandered loop antenna. Fig. 2(a) shows the detailed layout of the proposed matching network. The connection between the matching network and the meandered loop is achieved through a vertical metallic sheet as shown in Fig. 2(b). It has a width of 2.1 mm with a height of 1.51 mm. Layer 4 (foam) is embedded within the design to ensure the appropriate positioning of the vertical sheet and in order to allow the appropriate current flow between layer 3 and layer 5. Such flow is depicted in Fig. 2(b) for the two states of the integrated RF-MEMS.

The corresponding surface current distribution along the meandered loop and the three integrated vertical layers are presented in Fig. 2(c). When the switch is OFF, the antenna's effective electrical length is mainly due to the meandered loop length that is designed to operate at 760 MHz. In the ON state, the antenna's electrical length accounts for the meandered loop in addition to the three integrated vertical layers. Accordingly, the frequency of operation and the total effective length corresponds to the half-wavelength at 575 MHz.

One of the major elements to consider for ensuring the appropriate operation of the RF MEMS is the biasing network. To bias this switch, we resort to three 20 nH RF chokes that are shown in Fig. 1(b). These RF chokes contribute to the connection of the control pins of the switch to the power supply that is to be provided by a software-controlled microcontroller. One RF choke connects the control pin of the switch to a controlled power supply. Another RF Choke connects the switch voltage pin to a 2.7 Volts voltage supply. The last RF choke connects the ground pin of the switch to the ground plane of the antenna. The respective positions of the various RF chokes are shown in Fig. 1(b). Furthermore, Fig. 2(b) shows the current paths when the RF MEMS is either ON or OFF along with its appropriate biasing circuitry.

III. MEASUREMENTS AND RESULTS

Small antenna measurement techniques are implemented to ensure accurate measurement results [12], [13]. These techniques are based on incorporating a ferrite bead RF-choke and a balun between the antenna input terminal and the RF cable. The comparison between the simulated and measured reflection coefficients for both states of the RF-MEMS are shown in Fig. 3. In the OFF state, an operation at 760 MHz is obtained with a bandwidth of 3 MHz. While in the ON state, the antenna operates at 575 MHz with a bandwidth of 6 MHz. Such bandwidth is sufficient for the needed operation across the desired frequency bands.

Fig. 4 shows the antenna's simulated and measured radiation patterns when the switch is either in the OFF or ON states. The radiation patterns are plotted in the *x*-*z* and *y*-*z* plane cuts accordingly. The proposed design preserves an omnidirectional pattern, which is desired for cognitive radio applications in an emergency communication platform. Furthermore, the antenna preserves linear polarization in both its reconfiguration states. The radiation efficiency is found to be 40% at 575 MHz and 62% at 760 MHz. Such efficiencies are acceptable when designing ultra-compact antennas with a high-size reduction percentage as the one presented herein.

The compactness and efficiency of the proposed antenna are benchmarked using the figure of merit (FoM), shown in Eq. (1), and its calculated values are displayed in Table 1.

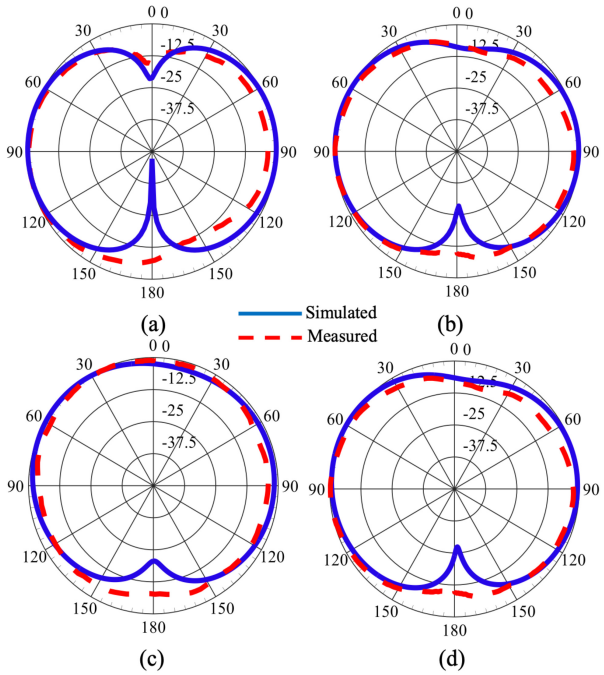

FIGURE 4. The simulated and measured radiation patterns (a) at 575 MHz in the *x-z* plane, (b) at 575 MHz in the *y-z* plane, (c) at 760 MHz in the *x-z* plane, (d) at 760 MHz in the *y-z* plane.

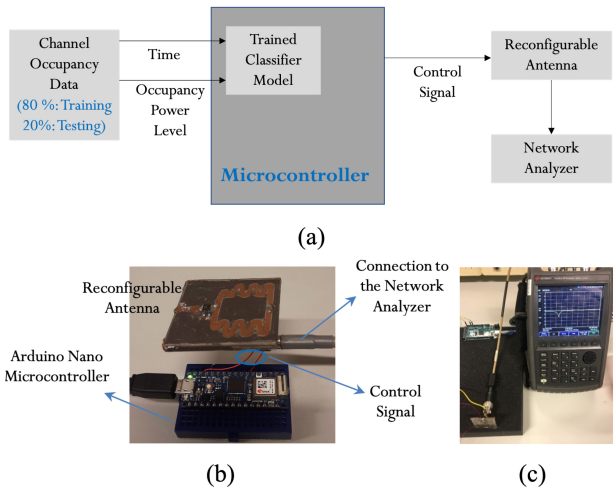

FIGURE 5. (a) The block diagram of the built classifier model to validate the operation of the proposed antenna structure in a cognitive radio environment, (b) The corresponding cognitive radio experimental setup showing how the Arduino microcontroller is controlling the biasing circuit of the RF-MEMS, (c) the antenna responding to the trained classifier and reconfiguring its frequency of operation.

The FoM is a function of the radiation efficiency (RE) and the normalized antenna volume which considers the active area of the antenna normalized to the cube of the largest wavelength.

$$FoM = \frac{RE}{100 \times \left(\frac{Volume_{Antenna}}{\lambda^3}\right)} \quad (1)$$

The obtained FoM for the proposed structure in comparison to other works in the literature is presented in Table 1. Such a result highlights the superior performance of the proposed design by maintaining acceptable efficiency values despite the extreme miniaturization aspect.

TABLE 1. Comparative table between the proposed design and other work available in the literature.

	Size	# Switches	Rad. Eff. (%)	FOM
[5]	0.41λx0.41λ x 0.04λ	0	63%@3.5GHz	0.94
[7]	0.145λx0.13λ x0.0192λ	1	35%@600MHz	9.67
[12]	0.28λx0.28λ x0.004λ	6	81% @ 2.4 GHz	25.82
[14]	0.135λx0.135λ x0.045λ	4	12.2% @ 860MHZ	1.49
This work	**0.11λx0.11λ x0.006λ**	**1**	**62%@760MHz 40%@575MHz**	**55.09**

IV. TESTING THE ANTENNA IN AN INTERWEAVE COGNITIVE RADIO ENVIRONMENT

To test the operation of the proposed reconfigurable antenna structure in a cognitive radio environment, a classifier model was built to automate and control the status of the integrated RF-MEMS according to the activity of the users in the channel. Such control enables the antenna to reconfigure its operating frequency based on the identified unoccupied channel. A block diagram detailing the proposed cognitive radio setup is shown in Fig. 5(a).

The classifier model is built by relying on synthetic data representative of UHF TV band usage [1] as a function of time and corresponding power levels. The data is chosen concerning the two operational frequency bands of the reconfigurable antenna at 565 MHz and 760 MHz respectively. In addition, the acquired data is divided as follows: 80% of the data is used to build and train the model while the remaining 20% is used for testing to monitor the reconfiguration of the proposed antenna structure. Accordingly, the model has two inputs as shown in Fig. 5(a). The first input is the time when the corresponding channel occupancy is recorded while the second input is the normalized power level of the band of interest at the previous time slot. The trained classifier model is then embedded within a microcontroller (*i.e.,* Arduino Nano 33 IoT board [15]) whose output controls the status of the integrated RF-MEMS within the reconfigurable antenna. The monitoring of the reconfiguration of the antenna structure is done by connecting it to a network analyzer and monitoring the corresponding reflection coefficient as depicted in Fig. 5(a) and Fig. 5(c).

The data used to represent the UHF band usage is divided into two sets based on the normalized power level within either band for a given time instance. The first set corresponds to the case where a given frequency band is occupied while the second set maps to the case where the frequency band is idle, and no one is using it. This is achieved by considering that the high level of the normalized RF power signifies the usage of the UHF band, whereas the level that is below the occupancy reference of the RF power signifies the availability of the channel. The occupancy reference level is obtained by computing the overall average power from the data used for training the model at the two frequency bands for all considered time instances. Accordingly, the "high

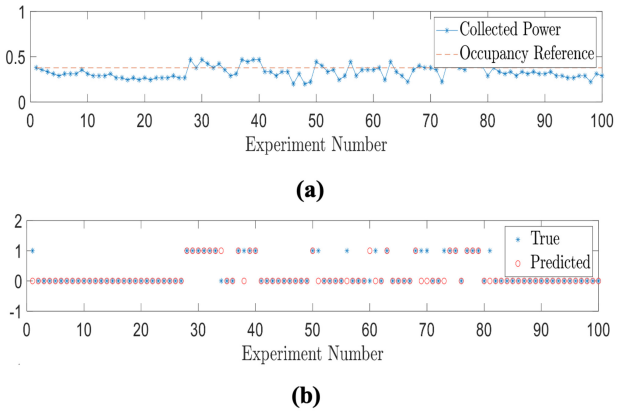

FIGURE 6. The occupancy power levels that are fed to the model to test its functionality in controlling the integrated switch within the reconfigurable antenna, (b) The prediction and the true outcome for the respective occupancy power levels.

power" slot is labeled with "1" while the "low power" slot is assigned a label of "0" for a given band and time slot. The experimental setup is shown in Fig. 5(b) and Fig. 5(c) where the trained model is fed to the microcontroller that controls the state of the RF-MEMS. The output of the microcontroller is fed to the biasing network of the switch where the microcontroller supplies the RF-MEMS with a voltage of 3.3V with a current of 2mA in the ON state.

To test the functionality of the trained model that is embedded within the Arduino Nano microcontroller, a new set of collected input data in terms of power levels at the previous time slots for different time instances is fed to the built model. The power levels that were fed to the microcontroller are shown in Fig. 6(a). These power levels are plotted with respect to the occupancy reference power level that was used during the training process of the classifier model. For each power level fed to the microcontroller, the trained model outputs a signal to control the status of the integrated switch within the proposed reconfigurable antenna. More specifically, the output of this algorithm is a supplied biasing voltage (V_{DD}) when the trained model predicts that the 760 MHz is occupied and that the 565 MHz band is not. This activates the RF-MEMS and leads to transmission at 565 MHz. The output is 0 volt to deactivate the switch when the prediction is that the 760 MHz is idle, thereby leading to transmission at 760 MHz. Therefore, the antenna changes its operating frequency depending on the pre-learned spectrum availability. If the trained model predicts that both channels are occupied, then it halts and waits for the next available slot and channel while executing continuous and cyclic monitoring.

Fig. 6(b) plots the predicted channel occupancy from the trained model. The built classifier model produces a 90% correct prediction outcome. This experimental setup shows the ability of the proposed antenna system to change its operating frequency depending on the pre-learned spectrum availability. Such spectrum availability can be updated dynamically and, on the go, to decide which state of the antenna to adopt and at which time. Hence, this protocol ensures the continuous operation of the antenna in an interweave cognitive radio platform and the appropriate suitability of such a component in a compact setup for dynamic communications systems.

V. CONCLUSION

In this paper, a novel compact reconfigurable multilayered folded antenna is designed. The antenna design relies on meandering and extreme folding. This has the advantage of reducing its size with extreme miniaturization aspects while ensuring its operation at UHF with acceptable radiation efficiencies. The antenna is fabricated and measured, and the measured results agree well with the simulated ones. In addition, the proposed reconfigurable antenna is tested in a cognitive radio scenario where the antenna is controlled by a pre-designed channel occupancy model to predict the channel availability at a certain time and in a certain area, proving its validity for operation in emergencies and areas with diminished communication infrastructure.

ACKNOWLEDGMENT

The authors would like to acknowledge the American University of Beirut, University Research Board for their support of this work.

REFERENCES

[1] "Voice and data coverage." Accessed: Mar. 2022. [Online]. Available: https://www.uscellular.com/coverage-map/coverage-indicator.html
[2] Y. Tawk, J. Costantine, and C. G. Christodoulou, "Cognitive-radio and antenna functionalities: A tutorial [wireless corner]," *IEEE Antennas Propag. Mag.*, vol. 56, no. 1, pp. 231–243, Feb. 2014.
[3] Y. Tawk, J. Costantine, and C. G. Christodoulou, *Antenna Design for Cognitive Radio*. Norwood, MA, USA: Artech House, 2016.
[4] F. A. Asadallah, A. Eid, G. Shehadeh, J. Costantine, Y. Tawk, and E. M. Tentzeris, "Digital reconfiguration of a single arm 3-D bowtie antenna," *IEEE Trans. Antennas Propag.*, vol. 69, no. 7, pp. 4184–4188, Jul. 2021, doi: 10.1109/TAP.2020.3044703.
[5] A. Boukarkar, X. Q. Lin, Y. Jian, L. Y. Nie, P. Mei, and Y. Q. Yu, "A miniaturized extremely close-spaced four-element dual-band MIMO antenna system with polarization and pattern diversity," *IEEE Antennas Wireless Propag. Lett.*, vol. 17, no. 1, pp. 134–137, Jan. 2018.
[6] X. Zhang, F. Sun, G. Zhang, and L. Hou, "Compact UHF/VHF monopole antennas for cubesats applications," *IEEE Access*, vol. 8, pp. 133360–133366, 2020, doi: 10.1109/ACCESS.2020.3008540.
[7] S. C. del Barrio, E. Foroozanfard, A. Morris, and G. F. Pedersen, "Tunable handset antenna: Enhancing efficiency on TV white spaces," *IEEE Trans. Antennas Propag.*, vol. 65, no. 4, pp. 2106–2111, Apr. 2017, doi: 10.1109/TAP.2017.2662221.
[8] F. A. Asadallah et al., "A miniaturized reconfigurable UHF antenna," in *Proc. IEEE Int. Symp. Antennas Propag.*, Jul. 2018, pp. 295–296.
[9] F. A. Asadallah, J. Costantine, and Y. Tawk, "Isolation enhanced MIMO PIFA system with multiple reconfiguration techniques," *IET Microw. Antennas Propag.*, vol. 14, no. 9, pp. 835–850, 2020.
[10] C. Balanis, *Modern Antenna Handbook*. Hoboken, NJ, USA: Wiley, 2015.
[11] A. Devices, "Wideband, 40 dB Isolation at 1 GHz, CMOS 1.65 V to 2.75 V, SPST Switches," Data Sheet ADG901/ADG902, Analog Devices, Wilmington, MA, USA, 2005.
[12] Z. Wang and Y. Dong, "Low-profile omnidirectional WIFI antennas with pattern reconfigurability inspired by meta-resonators," *IEEE Trans. Antennas Propag.*, vol. 68, no. 10, pp. 6935–6942, Oct. 2020.
[13] J. Volakis, C.-C. Chen, and K. Fujimoto, *Antennas: Miniaturization Techniques & Applications*, 1st ed. New York NY, USA: McGraw Hill, 2010.
[14] Z. Wang, Y. Dong, and T. Itoh, "Ultraminiature circularly polarized RFID antenna inspired by crossed split-ring resonator," *IEEE Trans. Antennas Propag.*, vol. 68, no. 6, pp. 4196–4207, Jun. 2020.
[15] "Arduino nano 33 IoT." Accessed: Mar. 2022. [Online]. Available: https: https://store.arduino.cc/usa/nano-33-iot-with-headers